Wave Damping due to Wooden Fences along Mangrove Coasts

Dao, Tung; Stive, Marcel J.F.; Hofland, Bas; Mai, Tri

DOI
10.2112/JCOASTRES-D-18-00015.1

Publication date
2018

Document Version
Final published version

Published in
Journal of Coastal Research

Wave Damping due to Wooden Fences along Mangrove Coasts

Authors: Dao, Tung, Stive, Marcel J.F., Hofland, Bas, and Mai, Tri

Source: Journal of Coastal Research, 34(6) : 1317-1327

Published By: Coastal Education and Research Foundation

URL: https://doi.org/10.2112/JCOASTRES-D-18-00015.1

Journal of Coastal Research	34	6	1317–1327	Coconut Creek, Florida	November 2018

Wave Damping due to Wooden Fences along Mangrove Coasts

Tung Dao[†‡], Marcel J.F. Stive[†]*, Bas Hofland[†], and Tri Mai[§]

[†]Faculty of Civil Engineering and Geosciences
Delft University of Technology
Delft 2628 CN, The Netherlands

[‡]Faculty of Marine Sciences
Hanoi University of Natural Resources and Environments
Bac Tu Liem, Hanoi, Vietnam

[§]Faculty of Coastal and Offshore Engineering
National University of Civil Engineering
Hai Ba Trung, Hanoi, Vietnam

www.cerf-jcr.org

www.JCRonline.org

ABSTRACT

Dao, T.; Stive, M.J.F.; Hofland, B., and Mai, T., 2018. Wave damping due to wooden fences along mangrove coasts. *Journal of Coastal Research,* 34(6), 1317–1327. Coconut Creek (Florida), ISSN 0749-0208.

In the Mekong Delta, as in many other mangrove settings, wooden fences are considered beneficial coastal structures to provide sheltering for mangrove replantation efforts by reducing waves and currents and promoting sedimentation. One of the most quantitative previous studies on fence-induced wave reduction offered a first understanding of relevant process parameters. The present application of the advanced numerical time-domain wave model SWASH increases this understanding substantially and explains previously unexplained phenomena that were encountered in this earlier study. The findings reveal that wave damping increases with increasing fence thickness and with increasing density of the woody material in the fences. It further shows that the transmitted wave height (represented by the transmission coefficient) is inversely proportional to the Ursell number, implying that nonlinear waves are damped more effectively.

ADDITIONAL INDEX WORDS: *Coastal erosion, Mekong Delta, SWASH model.*

INTRODUCTION

The Mekong River runs through five countries before reaching Vietnam, where it eventually bifurcates into nine river outlets, although presently only eight are left. It not only covers an area of 39,000 km^2 but also is home to nearly 17 million inhabitants in Southern Vietnam. Because erosion phenomena and mangrove losses have occurred at various locations along the Mekong Delta coast for the past few decades, many coastal structures, as well as coastal integrated management plans, have been built to provide coastal protection. Examples of coastal defenses along the coast are illustrated in Figure 1B.

Mangrove forests play a major role as coastal defenses given their capacity to dissipate waves and currents and to trap sediments and nutrients. The relevant hydrodynamic processes that are often described in the literature are waves and tidal flow. The capacity of mangrove forests to dissipate wave energy from storm surges and tsunamis is widely reported (*e.g.*, Alongi, 2008; Danielsen *et al.*, 2005; Othman, 1994; Phan *et al.*, 2015). The roots, trunks, and submerged canopies obstruct the orbital motion of the water particles, hindering the penetration of wave energy in the mangroves forests. Thus, a denser mangrove forest provides larger wave energy attenuation. The high friction generated by a mangrove fringe also causes a reduction in alongshore tidal flows, resulting in a net input of sediment inside a mangrove fringe (Truong, Ye, and Stive, 2017; Wattayakorn, Wolanski, and Kjerfve, 1990).

Unfortunately, a significant reduction of mangrove area has been observed in Southern Vietnam, causing severe erosion along the Mekong Delta coast. During the Vietnam War (1962–71), 40% of mangrove forests were eradicated (Hong and San, 1993), of which nearly 120,000 ha of about 600,000 ha of all mangrove-forest regions were lost because of defoliant use. With both natural regeneration and manual planning, mangrove forests had recovered gradually in 1975. However, timber overexploitation for charcoal and construction and conversion of forest into land use and aquaculture shrimp ponds again destroyed almost 50% of mangrove forests during the period 1980 to 2006 (*e.g.*, Christensen, Tarp, and Hjortso, 2008; Hong and San, 1993; Joffre and Schmitt, 2010; Nguyen *et al.*, 2013). For example, most original mangrove land was transformed into aquaculture land in 2015 along the Mekong Delta coast (Figure 1A). According to Duke *et al.* (2010), about 30 km of the mainland coast in Kien Giang was active and severe erosion from 2009 to 2010, leading to serious issues such as around 25 m of coastline in the Hon Dat district that retreated and 8 km of earthen dikes that partially eroded.

To protect valuable land from erosion, many coastal protection projects have been undertaken along the Mekong Delta coast (Figure 1B). A conventional Vietnamese approach to prevent storm surge, storm erosion, and chronic erosion has been to build solid structures, such as revetments (Figure 1B (1), (2)) and seawalls (Figure 1B (3)). However, from a coastal engineering perspective, such structures are not only technically challenging and cost intensive to apply (Schmitt and Albers, 2014) but also might negatively affect the sediment budget of the coast. Alternatively, salt marshes, combined with

DOI: 10.2112/JCOASTRES-D-18-00015.1 received 7 February 2018; accepted in revision 16 July 2018; corrected proofs received 13 September 2018; published pre-print online XX Month XXXX.
*Corresponding author: m.j.f.stive@tudelft.nl

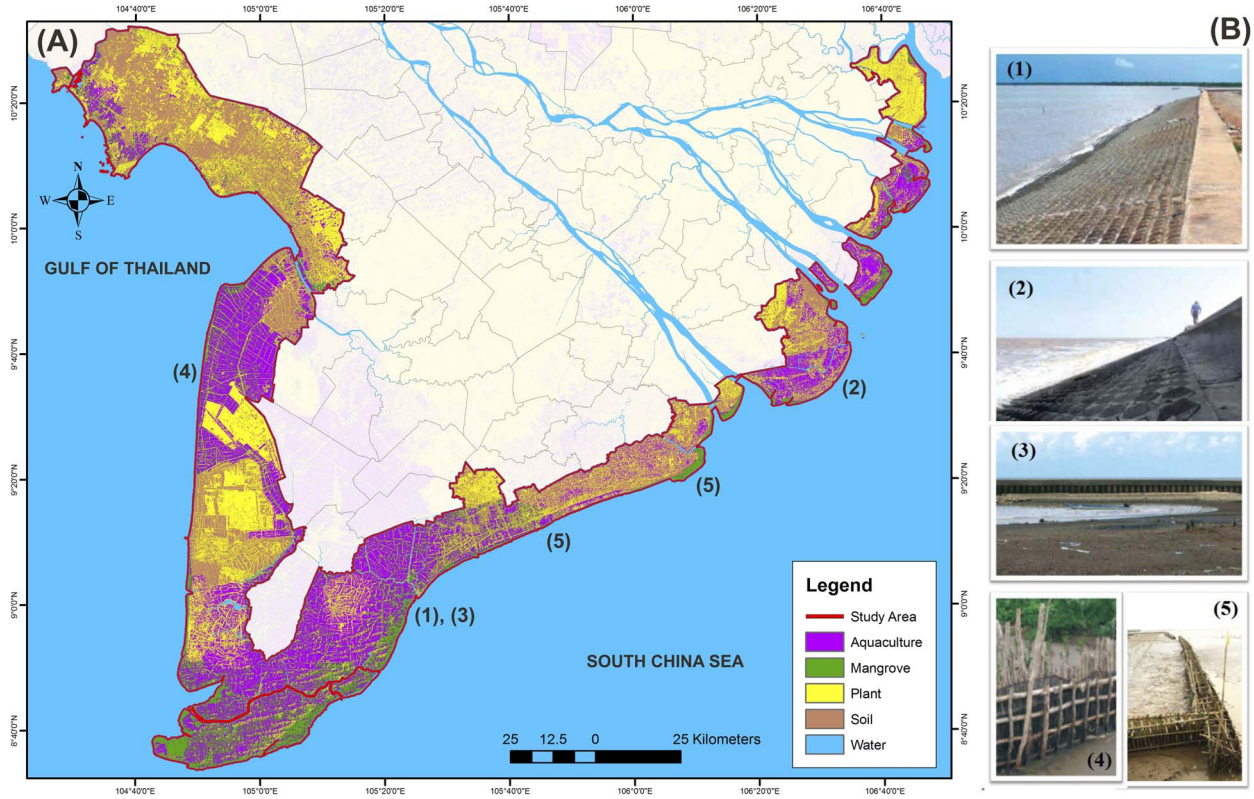

Figure 1. (A) Categories of land use along the Mekong Delta coast in 2015 (Phan, 2016). (B) Distribution of coastal defenses along the Mekong Delta coast. (1) and (2) Revetments at Ganh Hao, Bac Lieu Province (photo by GIZ Bac Lieu, 2013) and Tra Vinh Province (photo by Phuong Duong Thuy), respectively. (3) Seawall at Ganh Hao, Bac Lieu Province (photo by GIZ Bac Lieu). (4) Melaleuca barriers in Kien Giang province (Russell *et al*., 2012; photo by GIZ Kien Giang). (5) Bamboo fence at Nha Mat in Bac Lieu Province and Vinh Tan Commune, Soc Trang Province (photo by Tung Dao, 2016). (Color for this figure is available in the online version of this article.)

soft protection elements, such as brushwood and wooden poles (Figure 1B (4), (5)), could be considered instead of or complementary to hard structures to protect erosive coastlines. For example, soft coastal defenses have been applied since the 13th century along European estuarine and lagoon coasts. During the 13th and 14th centuries, severe storm surges caused massive land losses, but farmers living along the coast gradually reclaimed land losses by using accretion techniques, such as digging drainage ditches and building small dams in the early 16th century (Bakker *et al*., 2002). The purpose of land reclamations for agricultural cultivation continued until the 1940s to 1960s (Schmitt and Albers, 2014). After this, the governments of both Germany and the Netherlands took responsibility for land accretion, promoting sedimentation in brushwood-fenced tidal flat areas for safety against flooding (Dijkema, 1983). Present brushwood fencing in mangrove replantation projects is the mangrove counterpart of salt marsh recruitment, like the Dutch *kwelders* where brushwood fences have been used for ages to stimulate sedimentation. To stimulate the implementation of soft protection methods in the context of the Mekong Delta, Deutsche Gesellschaft für Internationale Zusammenarbeit (GiZ) sponsored two projects in the period 2008–14, *viz*. Management of Natural Resources in the Coastal Zone of Soc Trang Province, Vietnam, and Mangrove Rehabilitation in the Mekong Delta.

Hydrodynamics of the Mekong Delta Coast

The Mekong Delta coastal environment is historically classified as a tide-dominated environment; however, waves are increasingly becoming more effective than the tide (Ta *et al*., 2002). In the region of the South China Sea, also known as the East Sea, the tide has a semidiurnal character ranging from more than 2.0 m at mean tide to 4.0 m at spring tide. Along the coast, the tidal range reduces toward Ca Mau Cape and the number of tidal days and the diurnal characteristics increase (Phan *et al*., 2015). According to Hoang and Nguyen (2006), the NE monsoon is dominating in the winter (November–April) and the SW monsoon is dominant in the summer (May–October). During the SW monsoon, the average significant wave heights ($H_{s\ \mathrm{av}}$), are lower than 5.0 m (Figure 2A), and the average wave peak periods ($T_{p\ \mathrm{av}}$) are 6.0 seconds (Figure 2B). Meanwhile, maximum significant wave heights and peak periods ($H_{s\ \mathrm{max}}$ and $T_{p\ \mathrm{max}}$) correspond to 10.5 m and 11.5 seconds, respectively, in the NE monsoon (Figure 2).

The east of the Mekong Delta coast, Soc Trang coast, in particular, is a special coast with extremely gently sloping foreshores (1/30,000; Phan *et al*., 2015). Therefore, even though

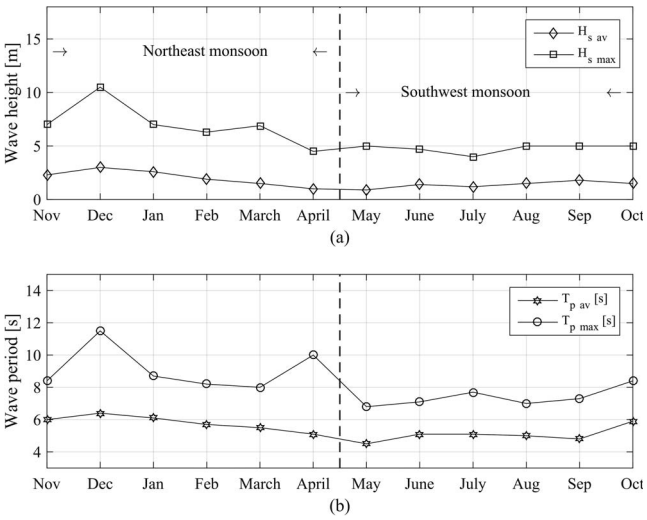

Figure 2. Monthly offshore wave characteristics at Bach Ho station (150 km offshore from the east side of the Mekong Delta coast, Figure 1A). Wave heights and periods were collected from 1986 to 2000 (Hoang and Nguyen, 2006).

waves from offshore can be large, this particular gentle and shallow foreshore causes a strong dissipation of the wave heights during wave propagations toward the shore because of breaking processes. Short waves with a frequency related to the primary wind waves lose substantial energy, while longer waves, such as swells and infragravity waves, are dissipated more slowly and can even exceed the short-wave heights in the nearshore (Phan *et al*., 2015).

Literature Review

Many studies have been carried out to investigate wave interaction with porous structures using numerical and physical models (Harada, Imamura, and Hiraishi, 2002; Sollitt and Cross, 1972). The initial waves seaward of a porous structure are composed of incident and reflected waves because of the interaction with the structure face. A small amount of wave energy will be lost because of breaking and dissipation inside the structure, and the remaining energy will be transmitted beyond the porous structure (Sollitt and Cross, 1972). Karim, Tanimoto, and Hieu (2004) conclude for vertical structures that structure width and porosity influence the amount of wave reflection and transmitted wave height, respectively. However, the preceding studies mostly consider small-scale experiments and a vertical orientation of the branches in the fence structure. The following focuses on studies of wave reduction due to porous fences using a particular material, such as melaleuca and bamboo, which is applied with a horizontal orientation.

Halide, Brinkman, and Ridd (2004) studied wave attenuation in vertical bamboo cylinder fields with widths varying from 15 to 90 m as the wave attenuator to protect mangrove forests. These authors used a numerical model to demonstrate the degree of wave dissipation within bamboo fields that have of a spatial density of 1, 2, and 4 cylinders per square meter and a bamboo diameter of 2, 4, and 8 cm, resulting in a porosity ranging from 90% to 96%. Their numerical model results confirmed the physical expectation that the larger the diameter and the denser the bamboo density, the larger the wave attenuation. These authors concluded that a bamboo field of 90 m with a spatial density of one pole of a 4-cm diameter per 1 m^2 was needed to achieve 50% incident wave attenuation. These authors scaled the spatial wave attenuation with the wavelength. However, the broader validity of this scaling was not explored.

Van Cuong *et al*. (2015) proposed applying a local wooden material melaleuca, used for housing and furniture, in fences as soft wave barriers. The purposes of these fences are to protect and increase sedimentation for young mangrove replantation along erosive shorelines in Kien Giang Province (Figure 1B (4)). The fences are assumed to decrease wave energy and thereby promote sedimentation of finer sediments and mud. Two designs were studied *in situ*. The basic design used a wave barrier fence 60 m offshore, consisting of two rows of melaleuca poles and bunches of tree branches and small-diameter poles between a 0.5-m gap. The other extended design used additional silt traps 20 m offshore that consisted of bamboo mats and fine fishing nets overlaying the seabed to increase sediment accretion rates. Whereas the impact of the melaleuca fences on sedimentation and survival of mangroves was indicated in detail, Van Cuong *et al*. (2015) only mentioned that the melaleuca fence immediately damped 56% of the incoming wave height. Three years of observation from 2009 to 2012 revealed significant mud accumulation in newly established mangrove seedling fields. The mud deposition inside the fenced areas increased significantly by 0.44 and 0.42 m in the basic design and the extended design, respectively. Unfortunately, there was no convincing evidence of wave datasets presented for wave reduction findings.

The strength and flexibility of bamboo and melaleuca differ distinctively. In developing countries, bamboo is used for household items and transport structures such as housing and bridges. From a coastal engineering point of view, the relatively cheap material bamboo has been shown to have superior strength and durability under strong wave conditions (Okubo, Fujii, and Yamamoto, 2004), while melaleuca can be destroyed easily under the same conditions. Research by Schmitt *et al*. (2013) and Albers, San, and Schmitt (2013) describes a site-specific approach for mangrove rehabilitation and replantation, in combination with bamboo breakwaters (bamboo T-fences), at erosive coasts in the Soc Trang Province, Vietnam (Figure 1B (5)). The following discussions concentrate on their study of wave damping through bamboo fences.

Using structures similar to the melaleuca fences, bamboo fences of two rows of vertical bamboo poles were investigated earlier in a wave flume with three main porosities of 4%, 16%, and 76% at a scale of 1:20 (Albers and Von Lieberman, 2011) to select the best design before deploying this at active erosion areas in the Vinh Tan Commune in Soc Trang Province. The selected design consisted of two rows of vertical 8-cm-diameter bamboo poles with the flexible and stiff brushwood inserted between the 40- to 50-cm gap of the pole rows to decrease the porosity (Figure 3).

Figure 3. Fence in the field (photo by Tung Dao, 2016). The brushwood was filled to the top of the fence at the beginning but eventually washed out by waves and currents. (Color for this figure is available in the online version of this article.)

To investigate wave transmission through bamboo fences, wave measurements were collected in a cross-shore profile section in which incident waves propagated perpendicularly to the fence in both laboratory and field experiments. Wave heights were collected at a distance approximately 5.0 m from the bamboo fence on both the landward and the seaward side. Following the literature on wave transmission through porous breakwaters, a transmission coefficient and a freeboard parameter were used to present the results. The transmission coefficient K_t is the ratio of transmitted wave height $H_{s,T}$ and total (incoming and reflected) initial wave height H_s:

$$K_t = \frac{H_{s,T}}{H_s} \tag{1}$$

The difference between incident wave height and initial wave height is discussed later in "Results." The freeboard R_c is the distance between still water level and fence crest (Figure 4). Fences can be submerged or emerged, represented by a negative or positive value of the relative freeboard, respectively.

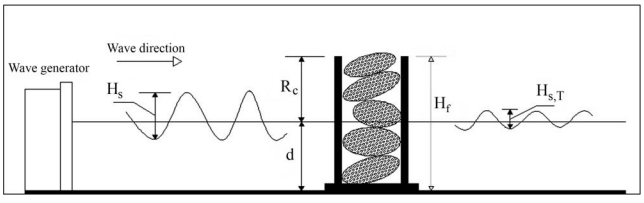

Figure 4. Physical modeling setup (Albers and Von Lieberman, 2011), where, $H_{s,T}$ and H_s are transmitted and initial wave heights, respectively. H_f is the fence height, and d is the water depth.

Schmitt *et al.* (2013) plotted the transmission coefficient K_t against the relative freeboard R_c/H_s, as shown in Figure 5. When the fences were well submerged, with the ratio R_c/H_s ranging from –2.5 to –1.0, wave heights reduced by 25% with stiff brushwood (blue lines) and by 30% with flexible brushwood (red lines). When the fence height increases, with the ratio R_c/H_s ranging from –1.0 to 6.0, the wave transmission rate decreases. For stiff brushwood, the transmission coefficient decreased linearly from 0.75 to 0.55 in the ratio R_c/H_s ranging from –1.0 to 1.0. For well-emerged fences ($R_c/H_s > 1$), the mean transmission coefficients were 0.55 and 0.3 for the stiff and the flexible brushwood, respectively. In the ratio R_c/H_s ranging from 1.5 to 3.0, the wave reduction has a scatter between 35% to 55% in the case of stiff brushwood. In addition, the physical modeling data (magenta diamonds) showed a larger reduction of wave height behind the fences. In the ratio R_c/H_s ranging from –1.5 to –1.0, wave heights reduced almost 0% ($K_t = 1.0$). In contrast, wave heights reduced by 80% to 90% in the ratio R_c/H_s ranging from 1.0 to 4.5. This is because of the relatively high density of the fences in comparison with the field (Albers, San, and Schmitt, 2013).

Whereas a first-order representation of wave damping because of wooden fences was described by presenting wave transmission as a function of relative freeboard and brushwood density, an explanation of second-order effects, as suggested by

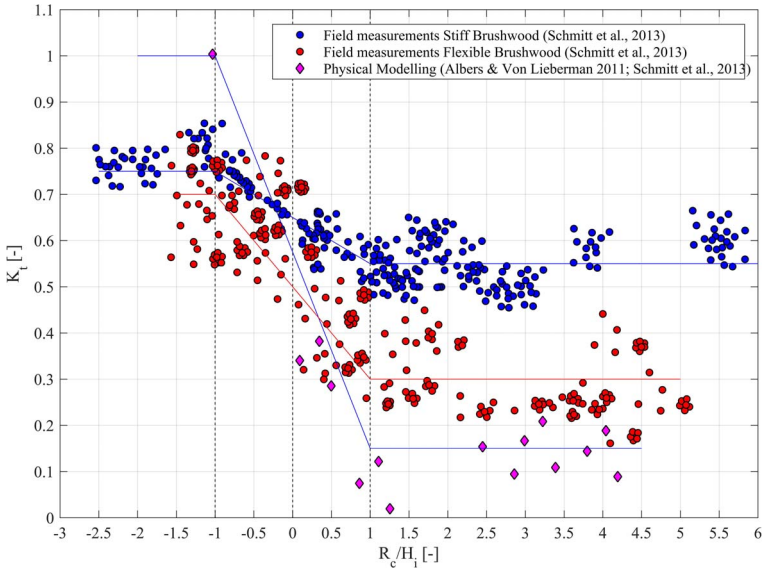

Figure 5. Wave transmission coefficient against relative freeboard; replotted after Schmitt *et al*. (2013). (Color for this figure is available in the online version of this article.)

the scatter clusters, remained intriguingly unknown. In Figure 5, the scatter clusters of stiff brushwood of K_t vary over small ranges of relative freeboard, and this variation is clearer than in other data sets, *e.g*., flexible brushwood, and physical experiments. It is hypothesized that other parameters such as wave nonlinearity, represented by a combination of wave steepness and relative water depth (the Ursell number; see "Results"), and fence thicknesses play a role. Although a snapshot of the significant wave height time series on the seaward and landward sides of the bamboo fence is presented, additional required parameters such as wave periods are not available.

In this study, therefore, a numerical time-domain wave model was validated and applied to test the mentioned hypotheses: (1) nonlinear waves are decreased more effectively, and (2) wave transmission depends on nondimensional fence thickness and increases with increasing relative thickness. The parameters used to investigate these hypotheses are wave nonlinearity and fence thickness made nondimensional by wavelength.

METHODS

After a description of the study site and the wooden fences in their local and international contexts, a numerical wave model is applied to investigate in more detail wave reduction due to the fences. In particular, the open-source model Simulating Waves till Shore (SWASH), various input parameters, and scenarios are introduced.

SWASH Model

SWASH is an advanced numerical, multidimensional time-domain model for simulating nonhydrostatic, free-surface flow based on the nonlinear shallow water equations (Zijlema, Stelling, and Smit, 2011). SWASH can accurately account for breaking processes in the nearshore (Smit, Zijlema, and Stelling, 2013).

The SWASH model is used for studying wave propagation in a cross-shore profile; hence, the governing equations are:

$$\frac{\partial u}{\partial x}+\frac{\partial w}{\partial z}=0 \qquad (2)$$

$$\frac{\partial \eta}{\partial t}+\frac{\partial}{\partial x}\int_{-d}^{\eta} u\,dz=0 \qquad (3)$$

$$\frac{\partial w}{\partial t}+\frac{\partial uw}{\partial x}+\frac{\partial ww}{\partial z}+\frac{1}{\rho}\frac{\partial (P_{\mathrm{nh}})}{\partial z}+\frac{\partial \tau_{zz}}{\partial z}+\frac{\partial \tau_{zx}}{\partial x}=0 \qquad (4)$$

$$\frac{\partial u}{\partial t}+\frac{\partial uu}{\partial x}+\frac{\partial wu}{\partial z}+\frac{1}{\rho}\frac{\partial (P_{\mathrm{h}}+P_{\mathrm{nh}})}{\partial x}+\frac{\partial \tau_{xz}}{\partial z}+\frac{\partial \tau_{xz}}{\partial x}=0 \qquad (5)$$

where, x is the horizontal coordinate and z is the upward coordinate relative to the still water level. u and w are horizontal and vertical velocities, respectively. η is the free surface elevation relative to the still water level, and t is the time. The pressure contribution P is separated into the hydrostatic pressure P_{h} and nonhydrostatic pressure P_{nh}. The turbulent stresses τ are calculated from a constant turbulent viscosity.

At the bottom boundary, a bottom stress is applied, following a quadratic friction law, as:

$$\tau_b=c_f\frac{U|U|}{\eta+d} \qquad (6)$$

where, U is the depth-averaged velocity; c_f is the friction coefficient, which is based on Manning's roughness coefficient n (Zijlema, Stelling, and Smit, 2011):

Table 1. *Input parameters for SWASH.*

Fence Thicknesses B_f (m)							Shallow Water Depth d (m)		
0.40	0.44	0.48	0.52	0.56	0.60	0.64	0.20	0.25	0.40
Wave Periods T_p (s)							Initial Wave Heights H_{m0} (m)		
1.4	1.6	1.7	1.8	2.0	2.1	2.3	0.03	0.06	0.08

$$c_f = \frac{n^2 g}{d^{1/3}} \tag{7}$$

In the horizontal direction, a spatial resolution (Δx) of 0.02 m was applied, which is about 1/100 of the peak wavelength L_p. Similar to the cross-shore direction, the vertical grid was set to three layers along with the Keller-box scheme (as a default setting) to increase wave dispersion accuracy (Zijlema and Stelling, 2005). A time step of 0.0001 second was employed (corresponding to a Courant number of approximately 0.3). In this study, the background viscosity was set to 3.10^{-4} m^2/s within three layers that accounted for all forms of resolved vertical mixing. A constant bottom friction coefficient of 0.002 was applied. Other default settings in SWASH were used as much as possible.

For the fencing setup, vegetation settings used for wave energy attenuation due to vegetation were applied. Wave energy attenuation by vegetation area is included as a drag force:

$$C_D = \left(\frac{1}{K_v} - 1\right) \frac{m\sqrt{\pi}}{(K_s - 1) N_v b_v \alpha H_{0,\mathrm{rms}}} \tag{8}$$

where, C_D, b_v, and N_v are the vegetation drag coefficient, the diameter, and the spatial density, respectively; H_{rms} is the root-mean-square wave height (in meters); m is the foreshore slope; α is the mean relative height coefficient; and K_v and K_S, presented as Equations (9) and (10), are the dissipation coefficient of vegetation and the shoaling coefficient following Green's Law, respectively:

$$K_s = d_0^{1/4} d^{1/4} \tag{9}$$

$$K_v = \frac{1}{1 + \frac{2\beta H_{0,\mathrm{rms}}}{m}\left(d_0^{1/4} d^{1/4} - 1\right)} \tag{10}$$

$$\beta = \frac{\alpha C_D b_v N_v}{2\sqrt{\pi}} \tag{11}$$

Assuming that wooden fences with a similarity to rigid vegetation settings can be considered, representing the fence properties through three main parameters, *viz*. the mean vegetation height as fence height H_f, the vegetation diameter D_f, and a spatial density N_v as the number of cylinders per square meter. The Albers and Von Lieberman (2011) experiment informed the idea of using porosity in realistic fence design, but the supported data of the fences is not available, a cross-sectional porosity of 60% can be only assumed, to receive higher ratio of wave transmission, as well as to avoid too much reflection. Since the porosity is applied and the chosen density is at 1600 cylinders per square meter and a cylinder diameter D_f of 0.01 m, various fence thicknesses B_f from 0.4 to 0.64 m can be applied in the simulation (Table 1). Fence height was applied at 0.25 m to define a mean vegetation height that was originally described with three layers (crow, stem, and root). Other parameters were set as default.

Input Parameters and Scenarios

The study by Phan *et al*. (2015) teaches that gentle foreshore slopes create unique conditions when reaching shallow water depths at the entrance of coastal mangrove fields. The gentle slopes dissipate the short-wave energy and increase the long-wave energy, such that at the entrance to the mangrove forest, these energies are of the same order of magnitude, and their negative correlation changes into a positive one (Roelvink and Stive, 1989). Unfortunately, it is virtually impossible to scale the extremely gentle slopes of the Mekong Delta in a wave flume, such as the one available in the Delft University of Technology in which experiments are being prepared for physical tests of wave attenuation through fences. The generation of free long waves, which is important on gentle slopes, is mimicked by forcing a wave train with bound long waves to break at a steep slope (Buckley *et al*., 2015; Smit, Zijlema, and Stelling, 2013; Tsai *et al*., 2005). Figure 6 describes the profile applied in SWASH at laboratory-scale dimensions. At the left side, a wave-generation boundary condition is applied using second-order wave theory to generate low-frequency waves. At the right side, a sponge layer is set to absorb all incoming waves and to avoid reflection of waves back to the fence.

Three water levels, including emerged and submerged cases, are considered. While the fence height H_f was held constant at 0.25 m, the different water levels create both emerged and submerged fences. Seven fence thicknesses B_f were used. Wave periods with a range from 1.4 to 2.3 seconds are based on the Joint North Sea Wave Project (JONSWAP) spectrum as default settings, and then for each scenario, the wave height H_{rm0} and still water level are kept constant. The input parameters are presented in Table 1; hence, 63 scenarios are simulated.

RESULTS

In the analysis of the simulation results, a cutoff frequency f_{cutoff} was used at 0.3 Hz to distinguish the short-wave frequency as $f_{\mathrm{sw}} \geq f_{\mathrm{cutoff}}$ and the long-wave frequency as $0.005 \leq f_{\mathrm{sw}} < f_{\mathrm{cutoff}}$. Input parameters were chosen as $H_{m0} =$ 0.08 m, $T_p = 2.1$ seconds, and $B_f = 0.6$ m for the comparison with and without a fence and for the comparison short waves and long waves. Subsequently, the effect of fences on the damping of nonlinear waves is discussed.

Wave Damping for Different Freeboards

Figure 7 describes the short-wave attenuation through a fence compared with the attenuation in the absence of a fence for three water levels, representing three freeboards. In general, waves start to break at $x = 15$ m after shoaling in

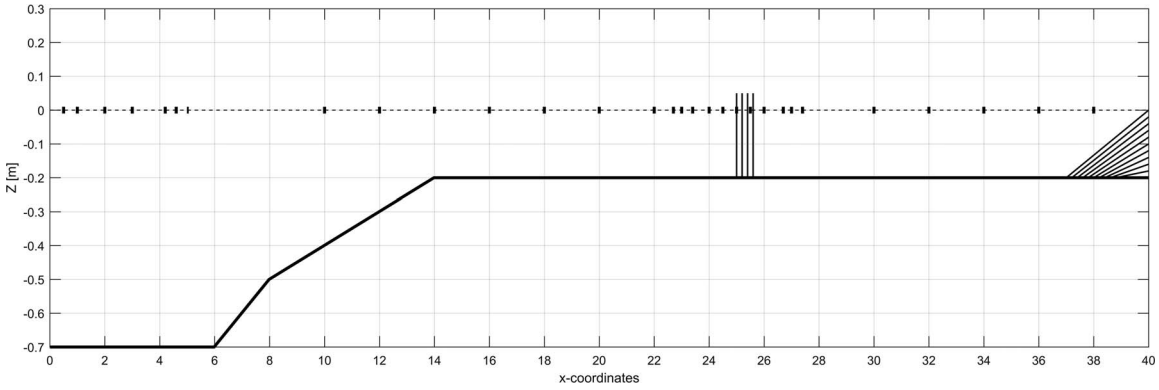

Figure 6. The SWASH profile presented at laboratory-scale dimensions. The wave maker and wave absorber are located at $x = 0$ m and $x = 37$ m, respectively. The fence is located at $x = 25$ m from seaward. The water level is at 0.7 m corresponding to emerged fences in deep part and is at 0.2 m in the shallow part. The crosses mark the 30 output points along the profile.

two cases. In the absence of a fence (solid line), incident short-wave heights $H_{s,I}$ gradually attenuate and dissipate at the sponge layer. With the appearance of the fences at $x = 25$ m, slight reflections occur in front of the fence. Following Goda and Suzuki (1976), the reflection coefficient is calculated as follows:

$$K_R = \sqrt{\left(H_s/H_{s,I}\right)^2 - 1} \tag{12}$$

Here the incident short-wave height $H_{s,I}$ was calculated from the case without a fence and the (total) initial wave height H_s; both incident and reflected wave heights were calculated from the case with a fence at $x = 20$ m (and thus outside the standing wave pattern). K_R was subsequently calculated for the chosen case. Reflected wave heights were 0.013, 0.027, and 0.02 m in water depths of 0.2, 0.25, and 0.4 m, respectively. Subsequently, reflection coefficients were 0.16, 0.32, and 0.24.

The evolution of the short-wave wave heights is shown in Figure 7. The transmitted wave height $H_{m0,T}$ decreases with the increase of water depth; for example, $H_{m0,T}$ reduces by roughly 30%, 20%, and 10% for water depths of 0.2, 0.25, and 0.4 m, respectively.

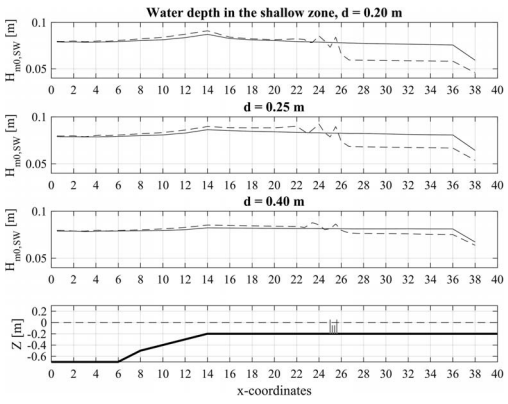

Figure 7. Short-wave height attenuation without a fence (solid line) and with a fence (dashed line) along the profile for three water levels: $H_{m0} = 0.08$ m, $T_p = 2.1$ s, $B_f = 0.6$ m.

Effects of Wave Nonlinearity and Fence Thickness on the Damping of Waves

The impact of a fence on reducing short waves is most simply indicated by the transmission coefficient K_t as defined by Equation (1). To calculate this coefficient, initial wave heights and transmitted wave heights were chosen at a location 5.0 m in front of and behind the fence following Schmitt *et al*. (2013). It is hypothesized that the more nonlinear the waves are, the stronger the damping is. To estimate the degree of nonlinearity of the waves, the combination of wave steepness and relative water depth (Doering and Bowen, 1995) is chosen as embedded in the Ursell number as:

$$U_r = \frac{H_{m0}L_p^2}{d^3} \tag{13}$$

where, H_{m0} is the initial significant wave height calculated by $H_{m0} = 4\sqrt{m_0}$, with m_0 as the zeroth order of moments. L_p and d are the peak wavelength and the water depth, respectively.

The transmission coefficient of short waves $K_{t\,\mathrm{SW}}$ in different water depths is plotted against the Ursell number in Figure 8. As can be seen, the transmission coefficient of short waves decreases linearly with the increase of Ursell number and relative fence thickness B_f/L_p. In particular, wave heights reduce up to 10% in the submerged case ($d = 0.4$ m) with a range of Ursell from 2 to 14 corresponding to B_f/L_p from 0.15 to 0.2. Larger wave reduction appears in emerged cases ($d = 0.2$ and 0.25 m) within a higher range of Ursell numbers from 6 to 30 and B_f/L_p from 0.2 to 0.32. In general, it can be said that the wave height reduces with the increase of the Ursell number and B_f/L_p; for example, the highest short-wave reduction of almost 30% is reached at the highest Ursell number of 30 and at the highest range of B_f/L_p from 0.28 to 0.32.

A second hypothesis is that the larger the ratio of relative fence thickness B_f/L_p, the stronger the wave damping. This hypothesis is strengthened by the grouping of the data in Figure 8 for B_f/L_p ratio ranges. By plotting the transmission coefficient against the product of the Ursell number and

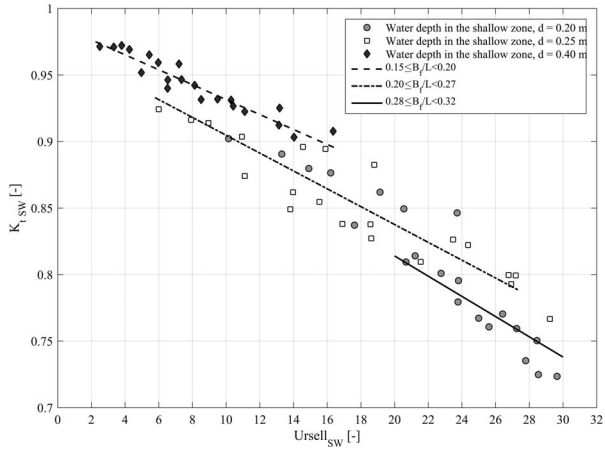

Figure 8. The relation of short-wave transmission coefficient and Ursell number for various classes of relative fence thickness.

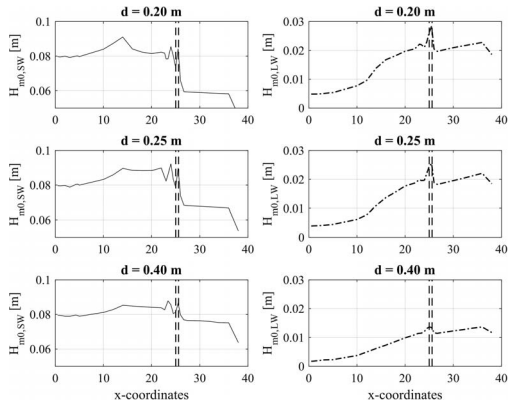

Figure 10. Significant short-wave heights $H_{m0,\mathrm{SW}}$ (solid line) and long-wave heights $H_{m0,\mathrm{LW}}$ (dash-dotted line) along the profile for three water levels. The fence located at $x = 25$ m is presented by the dashed line for $H_{m0} = 0.08$ m, $T_p = 2.1$ s, and $B_f = 0.6$ m.

dimensionless fence thickness, the joint effect of both fence thickness and nonlinearity on wave damping is revealed, suggesting a nearly linear correlation (Figure 9).

High-Frequency and Low-Frequency Wave Transformation

Significant short-wave heights $H_{m0,\mathrm{SW}}$ and long-wave heights $H_{m0,\mathrm{LW}}$ along the profile are presented for three water levels in Figure 10. In general, short waves and wave groups mostly dissipate and release free long waves from incident-bound long waves after breaking (Longuet-Higgins and Stewart, 1962). Up to the breaking point at $x = 14$ m, both short waves and long waves are increasing because of shoaling and are reflected slightly in front of the fence (at $x = 25$ m). While short waves reduce 30%, 20%, and 10% corresponding to the increase of water levels from 0.20 to 0.40 m in the shallow zone, the standing long-wave height pattern increases after passing through the fence.

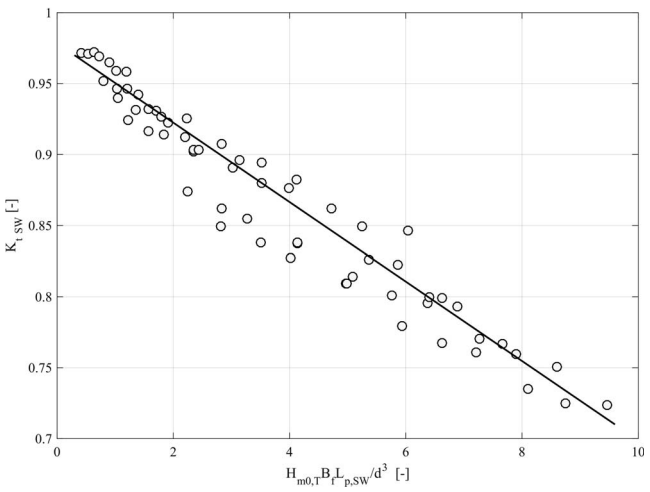

Figure 9. Relation of short-wave transmission coefficient and the product of Ursell number and fence thickness.

In conclusion, the results show that the amount of transmitted wave energy is affected not only by fence thicknesses but also by wave characteristics representing the nonlinearity degree. The more nonlinear the waves and the larger the ratio of B_f, the higher the short-wave reduction. For example, the maximum dissipation rate is 30% corresponding to the highest degree of Ursell number and the largest ratio of $B_f = 0.32$. Although the fence considerably affects the short waves, it shows minor effects on the long waves.

DISCUSSION

The freeboard R_c was used as a main parameter to explain wave reduction behind a fence by Schmitt *et al.* (2013). However, the reason for the large scatter of the transmission coefficient remained unknown. Therefore, the computation outputs were compared to their results in Figure 11, in which transmission coefficients are plotted against the relative freeboards.

From the simulation results (black–yellow circles), it appears that the reduction of short-wave heights increases proportionally with the decrease of water levels. Short-wave heights reduce 10% in the range of R_c/H_s from –5.5 to –1.5, in which the fence is greatly submerged. In contrast, when water levels are lower than the fence crest, the waves are more nonlinear because of shallow water effects, leading to an increase of wave reduction. This reduction increases from 5% to 30% in the range of R_c/H_s from –0.5 to 0.5, with a maximum 30% wave reduction for the largest nonlinear degree with the R_c/H_s approximate 0.5. However, there is an increase of transmission coefficient from 0.75 to 0.90 in the range of R_c/H_s from 0.5 to 1.5. This is because the positive value of the freeboard smaller wave heights becomes less nonlinear, leading to a small reduction, *i.e.* $K_t = 0.7$ at $R_c/H_s = 0.5$ compared with $K_t = 0.9$ at $R_c/H_s = 1.5$.

There are matching trends between the simulation results and the Schmitt *et al.* (2013) results. When the fence is greatly submerged corresponding to the range of R_c/H_s under –0.5,

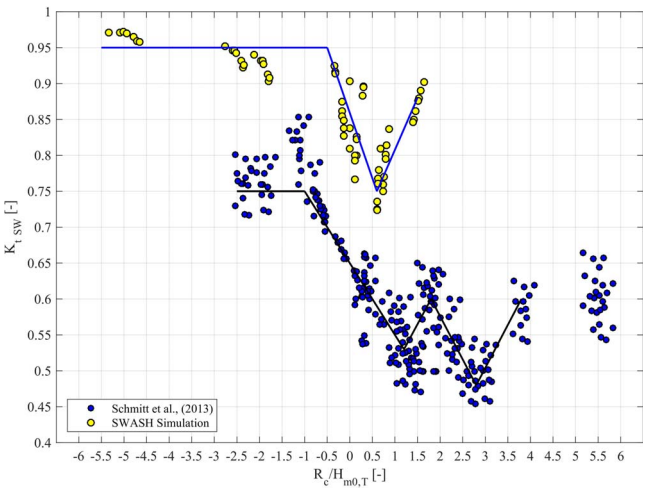

Figure 11. Simulation data (black–yellow circles) compared to field data for stiff brushwood (black–blue circles). (Color for this figure is available in the online version of this article.)

wave heights decrease slightly by about 10% for both the simulations and the Schmitt *et al*. (2013) results. In the range of R_c/H_s of –1.0 to 1.0, wave reduction from both simulations and field measurement reduces steeply about 25%, *e.g*., the reduction is from 95% to 70% for the simulations and from 75% to 50% for the stiff brushwood. Then, an increase of transmission coefficient of 0.1 occurs in the range of R_c/H_s from 0.5 to 1.5, *e.g*., K_t increases from 0.75 to 0.85 for the simulation and from 0.5 to 0.6 for the stiff brushwood. However, the amounts of wave reduction from the simulations are nearly 30% less than those of Schmitt *et al*. (2013), most likely because of the bottom friction effect. The applied bottom friction in SWASH is smaller than a realistic friction in the Mekong Delta. When fences are greatly submerged, the wave reduction for wave measurement is 20% more than in the simulation. It is obvious that for the emerged fence case, wave reduction in reality is still higher than in the simulations.

As mentioned in the literature review, both Van Cuong *et al*. (2015) and Schmitt *et al*. (2013) attempted to formulate a site-specific management approach for mangrove replantation at erosional sites. However, the role of sediment transport is not discussed. Long waves have been recognized as an important controlling factor for net sediment transport (Baldock, Manoonvoravong, and Pham, 2010). This net transport is proportional to the odd moment $<u|u|^2>$ (Bosboom and Stive, 2012), where, u is the velocity close to the bed consisting of a time-averaged velocity ($\bar{u}$), a short-wave averaged oscillatory motion of short waves (u_{SW}), and low-frequency motion at wave-group scale (u_{LW}). The term u^2 is related to the sediment concentration stirred up by the oscillatory wave motion and is proportional to the wave height in the shallow water. In the photo taken at Nha Mat in Bac Lieu Province coast during the flood (Figure 12), shorter waves, appearing farther offshore, were mostly obstructed by the bamboo fence placed just inshore of the building, while longer waves continued passing through until reaching the coast. These long waves may play a major role for a net import of sediment into the fenced site. Future work will focus on this mechanism and the role of long waves.

Figure 12. Wave patterns behind a wooden fence at Nha Mat in Bac Lieu Province (photo by Tung Dao, 2016). The bamboo fence is located parallel to the coast and just inshore of the building. (Color for this figure is available in the online version of this article.)

CONCLUSIONS

In the Mekong Delta, as in many other mangrove settings, wooden fences are considered beneficial coastal structures to provide sheltering for mangrove replantation efforts by reducing waves and currents and promoting sedimentation. The study from Schmitt *et al*. (2013) reveals a wave reduction behind fences as much as 50%. Their analysis introduces the freeboard parameter R_c as a prime parameter to explain fence-induced wave reduction. However, the degree of wave nonlinearity and the nondimensional fence thickness are more important parameters for dimensionless freeboards.

The transmitted wave height decreases with the increase of the Ursell number and the relative fence thickness B_f/L_p. When the Ursell number is below 16, the wave transmission coefficient varies from 0.95 to 0.90 for the range of B_f/L_p from 0.15 to 0.20 for submerged cases. With higher Ursell numbers from 16 to 30, K_t varies from 0.85 to 0.70 for the emerged cases.

Schmitt *et al*. (2013) use only the freeboard R_c as an important parameter, inspired by wave transmission over permeable structures. The present results reveal the importance of other parameters, *i.e*. the wave nonlinearity and the relative fence thickness. In addition, fence porosity may affect wave damping. Future work will focus on this parameter.

Fences can reduce short waves effectively, whereas they only yield a minor effect on long waves. Even though it is hypothesized that highly nonlinear waves are damped effectively, long waves are still the exception and this will be studied in future work.

ACKNOWLEDGMENTS

The Delft University of Technology, the Netherlands; the Ministry of Education and Training, Vietnam International Education Cooperation Department, Vietnam; and Hanoi University of Natural Resources and Environments, Hanoi, Vietnam, support this research. The permitted use of the data by Professor Thorsten Albers, Lieberman GmbH, von Lieberman Consulting Engineers, University of Applied Sciences Bremerhaven, is gratefully acknowledged.

LITERATURE CITED

Albers, T. and Von Lieberman, N., 2011. *Current and Erosion Modelling Survey*. Eschborn, Germany: Deutsche Gesellschaft für Internationale Zusammenarbeit (GiZ), 61p.

Albers, T.; San, D.C., and Schmitt, K., 2013. *Shoreline Management Guidelines: Coastal Protection in the Lower Mekong Delta*. Eschborn, Germany: Deutsche Gesellschaft für Internationale Zusammenarbeit (GiZ), 124p.

Alongi, D.M., 2008. Mangrove forests: Resilience, protection from tsunamis, and responses to global climate change. *Estuarine, Coastal and Shelf Science,* 76(1), 1–13.

Bakker, J.P.; Esselink, P.; Dijkema, K.S.; Van Duin, W.E., and De Jong, D.J., 2002. Restoration of salt marshes in the Netherlands. *Hydrobiologia,* 478(1–3), 29–51. doi:10.1023/A:1021066311728.

Baldock, T.E.; Manoonvoravong, P., and Pham, K.S., 2010. Sediment transport and beach morphodynamics induced by free long waves, bound long waves and wave groups. *Coastal Engineering,* 57(10), 898–916. doi:10.1016/j.coastaleng.2010.05.006.

Bosboom, J. and Stive, M.J.F., 2012. *Coastal Dynamics I*. Lectures Notes *CIE4305*. Delft, The Netherlands: VSSD, 584p.

Buckley, M.L.; Lowe, R.J.; Hansen, J.E., and Van Dongeren, A.R., 2015. Dynamics of wave setup over a steeply sloping fringing reef. *Journal of Physical Oceanography,* 45(12), 3005–3023.

Christensen, S.M.; Tarp, P., and Hjortso, C.N., 2008. Mangrove forest management planning in coastal buffer and conservation zones, Vietnam: A multimethodological approach incorporating multiple stakeholders. *Ocean and Coastal Management,* 51(10), 712–726. doi:10.1016/j.ocecoaman.2008.06.014.

Danielsen, F.; Sorensen, M.K.; Olwig, M.F.; Selvam, V.; Parish, F.; Burgess, N.D.; Hiraishi, T.; Karunagaran, V.M.; Rasmussen, M.S., and Hansen, L.B., 2005. The Asian tsunami: A protective role for coastal vegetation. *Science (Washington),* 310(5748), 643.

Dijkema, K.S., 1983. Use and management of mainland salt marshes and Halligen. *In:* Dijkema, K.S. and Wolff, W.J. (eds.), *Flora and Vegetation of the Wadden Sea Islands and Coastal Areas*. Rotterdam, The Netherlands: Balkema, pp. 302–312.

Doering, J.C. and Bowen, A.J., 1995. Parametrization of orbital velocity asymmetries of shoaling and breaking waves using bispectral analysis. *Coastal Engineering,* 26(1–2), 15–33.

Duke, N.; Wilson, N.; Mackenzie, J.; Nguyen, H.H., and Puller, D., 2010. *Assessment of Mangrove Forests, Shoreline Condition and Feasibility for REDD in Kien Giang Province, Vietnam*. Eschborn, Germany: Deutsche Gesellschaft für Technische Zusammenarbeit (GTZ), 128p.

Goda, Y. and Suzuki, Y., 1976. Estimation of incident and reflected waves in random wave experiments. *Proceedings of the 15th International Conference on Coastal Engineering* (Honolulu, Hawaii), pp. 828–845. doi:10.1061/9780872620834.048.

Halide, H.; Brinkman, R., and Ridd, P., 2004. Designing bamboo wave attenuators for mangrove plantations. *Indian Journal of Marine Sciences,* 33(3), 220–225.

Harada, K.; Imamura, F., and Hiraishi, T.L., 2002. Experimental study on the effect in reducing tsunami by the coastal permeable structures. *Proceedings of the 12th International Offshore and Polar Engineering Conference* (International Society of Offshore and Polar Engineers), pp. 652–658.

Hoang, V.H. and Nguyen, H.N., 2006. Result on study of wave field on Dong Nai, Sai Gon estuaries and suggestion of sea bank and river mouth protection methods. *Proceedings of the Vietnam–Japan Estuary Workshop in Collaboration between Tohoku University and Water Resources University,* pp. 140–150.

Hong, P.N. and San, H.T., 1993. *Mangroves of Vietnam*. Bangkok, Thailand: IUCN, 170p.

Joffre, O.M. and Schmitt, K., 2010. Community livelihood and patterns of natural resources uses in the shrimp-farm impacted Mekong Delta. *Aquaculture Research,* 41(12), 1855–1866.

Karim, M.F.; Tanimoto, K., and Hieu, P.D., 2004. Simulation of wave transformation in vertical permeable structure. *International Journal of Offshore and Polar Engineering,* 14(2), 729–735.

Longuet-Higgins, M.S. and Stewart, R.W., 1962. Radiation stress and mass transport in gravity waves, with application to "surf beats." *Journal of Fluid Mechanics,* 13(4), 481–504. doi:10.1017/S0022112062000877.

Nguyen, H.-H.; McAlpine, C.; Pullar, D.; Johansen, K., and Duke, N.C., 2013. The relationship of spatial–temporal changes in fringe mangrove extent and adjacent land-use: Case study of Kien Giang coast, Vietnam. *Ocean & Coastal Management,* 76, 12–22.

Okubo, K.; Fujii, T., and Yamamoto, Y., 2004. Development of bamboo-based polymer composites and their mechanical properties. *Composites Part A: Applied Science and Manufacturing,* 35(3), 377–383. doi:10.1016/j.compositesa.2003.09.017.

Othman, M.A., 1994. Value of mangroves in coastal protection. *Hydrobiologia,* 285(1–3), 277–282.

Phan, L.K.; van Thiel de Vries, J.S.M., and Stive, M.J.F., 2015. Coastal mangrove squeeze in the Mekong Delta. *Journal of Coastal Research,* 31(2), 233–243. doi:10.2112/JCOASTRES-D-14-00049.1.

Phan, M.H., 2016. Dynamics of mangrove in lower Mekong Delta. Delft, The Netherlands: Delft University of Technology, dataset. doi:10.4121/uuid:da314d82-83f6-46d9-bdf6-a37f48d24326.

Roelvink, J.A. and Stive, M.J.F., 1989. Bar-generating cross-shore flow mechanisms on a beach. *Journal of Geophysical Research: Oceans,* 94(C4), 4785–4800.

Russell, M.; Michaels, K.; Dart, P.; Duke, N., and To, H.H., 2012. Coastal rehabilitation and mangrove restoration using melaleuca fences: Practical experience from Kien Giang province. Eschborn,

Germany: Deutsche Gesellschaft fur Internationale Zusammenarbeit (GiZ), 26p.

Schmitt, K. and Albers, T., 2014. Area coastal protection and the use of bamboo breakwaters in the Mekong Delta. *In:* Thao, N.D.; Takagi H., and Esteban, M. (eds.), *Coastal Disasters and Climate Change in Vietnam: Engineering and Planning Perspectives*. London: Elsevier, pp. 107–132. doi:10.1016/B978-0-12-800007-6.00005-8.

Schmitt, K.; Albers, T.; Pham, T.T., and Dinh, S.C., 2013. Site-specific and integrated adaptation to climate change in the coastal mangrove zone of Soc Trang Province, Viet Nam. *Journal of Coastal Conservation,* 17(3), 545–558.

Smit, P.; Zijlema, M., and Stelling, G., 2013. Depth-induced wave breaking in a non-hydrostatic, near-shore wave model. *Coastal Engineering,* 76, 1–16. doi:10.1016/j.coastaleng.2013.01.008.

Sollitt, C.K. and Cross, R.H., 1972. Wave transmission through permeable breakwaters. *Proceedings of the 13th International Conference on Coastal Engineering* (Vancouver, Canada), pp. 1827–1846. doi:10.1061/9780872620490.106.

Ta, T.K.O.; Nguyen, V.L.; Tateishi, M.; Kobayashi, I.; Saito, Y., and Nakamura, T., 2002. Sediment facies and Late Holocene progradation of the Mekong River Delta in Bentre Province, southern Vietnam: An example of evolution from a tide-dominated to a tide- and wave-dominated delta. *Sedimentary Geology,* 152(3), 313–325.

Truong, S.H.; Ye, Q., and Stive, M.J.F., 2017. Estuarine mangrove squeeze in the Mekong Delta, Vietnam. *Journal of Coastal Research,* 33(4), 747–763. doi:10.2112/JCOASTRES-D-16-00087.1.

Tsai, C.-P.; Chen, H.-B.; Hwung, H.-H., and Huang, M.-J., 2005. Examination of empirical formulas for wave shoaling and breaking on steep slopes. *Ocean Engineering,* 32(3–4), 469–483.

Van Cuong, C.; Brown, S.; To, H.H., and Hockings, M., 2015. Using melaleuca fences as soft coastal engineering for mangrove restoration in Kien Giang, Vietnam. *Ecological Engineering,* 81, 256–265. doi:10.1016/j.ecoleng.2015.04.031.

Wattayakorn, G.; Wolanski, E., and Kjerfve, B., 1990. Mixing, trapping and outwelling in the Klong Ngao mangrove swamp, Thailand. *Estuarine, Coastal and Shelf Science,* 31(5), 667–688.

Zijlema, M. and Stelling, G.S., 2005. Further experiences with computing non-hydrostatic free-surface flows involving water waves. *International Journal for Numerical Methods in Fluids,* 48(2), 169–197.

Zijlema, M.; Stelling, G., and Smit, P., 2011. SWASH: An operational public domain code for simulating wave fields and rapidly varied flows in coastal waters. *Coastal Engineering,* 58(10), 992–1012.